Modeling Binding Modes of α7 Nicotinic Acetylcholine Receptor with Ligands: The Roles of Gln117 and Other Residues of the Receptor in Agonist Binding

Xiaoqin Huang[†], **Fang Zheng**[†], **Clare Stokes**[‡], **Roger L. Papke**[‡], and **Chang-Guo Zhan**[*,†]

Department of Pharmaceutical Sciences, College of Pharmacy, University of Kentucky, 725 Rose Street, Lexington, Kentucky 40536; Department of Pharmacology and Therapeutics, College of Medicine, University of Florida, Gainesvlle, Florida 32610

Abstract

Extensive molecular docking, molecular dynamics simulations, and binding free energy calculations have been performed to understand how α7-specific agonists of nicotinic acetylcholine receptor (nAChR), including AR-R17779 (**1**), GTS-21 (**4**), and 4-OH-GTS-21 (**5**), interact with the α7 receptor, leading to important new insights into the receptor–agonist binding. In particular, the cationic head of **4** and **5** has favorable hydrogen bonding and cation–π interactions with residue Trp149. The computational results have also led us to better understand the roles of Gln117 and other residues in the receptor binding with agonists. The computational predictions are supported by data obtained from wet experimental tests. The new insights into the binding and structure–activity relationship obtained from this study should be valuable for future rational design of more potent and selective agonists of the α7 receptor.

Introduction

Nicotinic acetylcholine receptors (nAChRs)[a] are important members of the Cys-loop superfamily of pentameric ligand-gated ion channels in the central nervous system (CNS).[1] These receptors directly mediate a broad range of brain functions such as learning and memory. Abnormal opening-and-closing of nAChRs contributes to neurodegenerative disorders, resulting in severe diseases such as Alzheimer's disease, Parkinson's disease, dyskinesias, Tourette's syndrome, and schizophrenia.[2] Among all the subtypes identified to date, α7 and α4β2 have been established as two major targets mediating the pathology of these severe diseases.[3-5] Compared to other nAChRs, the α7 receptor mediates the neuron-protective action of nicotine-like agonists against various stresses including β-amyloid and nerve growth factor depletion.[6-9] Selective α7 agonists can prevent receptor activation by β-amyloid$_{1–42}$ and do not possess significant drug dependence, making α7 receptor as a potential target for the treatment of Alzheimer's disease.[7,10,11] Hence, it is very interesting to design and discover novel, potent, and selective agonists of α7 nAChR.

[*]To whom correspondence should be addressed. Phone: 859-323-3943. Fax: 859-323-3575. zhan@uky.edu..
[†]Department of Pharmaceutical Sciences, College of Pharmacy, University of Kentucky.
[‡]Department of Pharmacology and Therapeutics, College of Medicine, University of Florida.

[a]Abbreviations: nAChR, nicotinic acetylcholine receptor; CNS, central nervous system; LBD, ligand binding domain; RESP, restrained electrostatic potential; AChBP, acetylcholine-binding protein; LGA, Lamarkian genetic algorithm; MD, molecular dynamics; PME, particle mesh Ewald.

(−)-Spiro[1-azabicyclo(2.2.2)octane-3,5′-oxazolidin-2′-one] (AR-R17779, **1**)[12,13] is a conformationally rigid analogue of acetylcholine and is a full agonist of α7 nAChR. **1** is highly selective for α7 nAChR over α4β2 and other nAChR subtypes. Preliminary structure-activity relationship revealed that the structure of this molecule is rather rigid and cannot bear structural changes (compounds **2** and **3** in Table 1) without losing its high affinity of binding with α7 nAChR. The unique potency and selectivity of **1** make this compound an important agent for understanding the structure and function of the α7 receptor. Another ligand, 3-[(2,4-dimethoxy)benzylidene]-anabaseine (GTS-21, **4**),[14] originally derived from the animal toxin anabaseine, has been tested as a partial agonist of α7 nAChR (Table 1), whereas it is a moderate antagonist of α4β2 nAChR.[7,15-18] This ligand (**4**) has demonstrated promising characteristics during the phase I clinical trials, i.e., enhancing a variety of cognitive behavior, much less toxic than nicotine, and large-dose administration without adverse effects.[19-21] Interestingly, **4** is easily metabolized by hepatic cytochrome P450. The primary metabolites are 2-OH, 4-OH, and 2,4-diOH-GTS-21.[22] Only 4-OH-GTS-21 (**5**)[22] displayed a little higher affinity than **4** for stimulating α7 receptors. Experimental studies also demonstrated that the protonation of the tetrahydropyridyl nitrogen is essential for the high-affinity binding of **4** and its metabolites with α7 nAChR. [17,18,22]

Contemporary understanding of the structure–function relationship of nAChRs has greatly benefited from the two major breakthroughs achieved so far, i.e., the refined structure of Torpedo α1β1δγ nAChR[23,24] and several crystal structures of the acetylcholine-binding protein (AChBP) in different agonist/antagonist-bound states.[25,26] Although the refined structure of α1β1δγ nAChR at 4 Å resolution has provided fundamental insights into the architecture of extracellular ligand binding domain (LBD) and the channel pore,[23] the binding site is obviously distorted, making it impossible to offer in-depth information about ligand binding. Overall, AChBP shares ~24% sequence identity with LBD of a nAChR and has the same pentameric assembly.[24] The X-ray crystal structure of agonist-bound AChBP has been recognized as the most appropriate template to model the LBD of nAChR for the purpose of studying the molecular mechanism of receptor–ligand interactions.[25-28] This progress has also paved the way to understand particular contributions from residues at a binding site to ligand binding. In our previous studies,[29,30] we proposed that Gln117,[31] a hydrophilic residue at the complementary side of the binding site, contributes important hydrogen bonding interaction to **1** binding with α7 nAChR and, thus, enhanced the subtype selectivity of **1** binding with nAChRs. It is notable that the agonist activities of **4** and **5** with α7 nAChR are close to that of **1**.[12,13,18,19] However, the structures of these compounds are quite different, which implies that **4** and **5** might interact with the α7 receptor in a significantly different binding mode compared to the **1** binding.[30]

The present study aims to understand how **4** and **5** bind with α7 nAChR and to better understand the role of Gln117 in α7 nAChR binding with different agonists. For this purpose, we first examined how wild-type α7 nAChR and its Gln117Phe mutant bind with a series of agonists and calculated the corresponding binding free energies. The obtained binding structures and binding free energies demonstrate the effects of the possible hydrogen bonding with Gln117 and other residues of α7 nAChR on the receptor binding with agonists. The calculated results predict that the roles of Gln117 in α7 nAChR binding with different agonists are different. The computational predictions are supported by data obtained from wet experiments and provide new receptor–agonist binding and structure–activity relationship (SAR) insights valuable for future rational design of novel agonists that can more potently and selectively interact with α7 nAChR.

Experimental Methods

Preparation of Molecular Structures

Geometries of protonated structures of five agonists, i.e., **1**–**5** in Table 1, were fully optimized by using Gaussian03 program32 at the HF/6-31+G(d) level. The atomic charges of all these protonated structures were derived from the first-principles electrostatic structure calculations at the HF/6-31+G(d) level as the restrained electrostatic potential (RESP) charges determined by using the standard RESP procedure implemented in the Antechamber module of the Amber8 program.33 The similar RESP-fitting calculations based on the first-principles electronic structure method were used in our previous computational studies of other protein–ligand systems and led to satisfactory binding structures.34‑38 The modeling of the mutant structure of human α7 nAChR in this study was based on the use of our previously modeled structure of ligand-binding domain (LBD) of wild-type human α7 nAChR.30 As the template used to model the LBD is the X-ray crystal structure25 of AChBP with an agonist (i.e., nicotine) bound in the binding site, the modeled LBD structure is expected to be close to that of the open-channel state of the α7 receptor but may also be related to the desensitized state. The constructed initial LBD structure was carefully energy-minimized by using the Sander module of the Amber8 program33 with a nonbonded cutoff of 10 Å, a conjugate gradient minimization method and convergence criterion of 0.01 kcal mol^{-1} Å^{-1}.

Molecular Docking and Molecular Dynamics Simulations

On the basis of the modeled LBD structures of wild-type human α7 receptor and its Gln117Phe mutant, molecular docking was performed for all of the considered agonists. Our docking studies were first performed for **5** binding with the wild-type α7 receptor and then extended to other receptor–agonist binding. Using the AutoDock 3.0.5 program,39 the agonist was docked into the binding site at the interface of two subunits of the LBD structure. During the docking process, the conformational search was performed using the Solis and Wets local search method,40 and the Lamarkian geneticalgorithm(LGA)39 was applied to deal with the receptor–ligand interactions. Among a series of docking parameters, the grid size was set at $60 \times 60 \times 60$, and the grid space used was the default value of 0.375 Å. As recommended by the AutoDock 3.0.5 programmer, the translational step size was set as 0.2 Å, while the step size for both quanternion and torsional change was 5°. For the LGA, parameters, the maximum number of energy evaluations was increased to 1800000. The docked receptor–ligand complex structures were ranked according to the calculated interaction energies combined with geometric matching quality. By visually checking the geometric matching quality of the docked binding structures with the lower binding energies, candidate structures that are consistent better with the known structure–activity relationships of α7 receptor agonists were compared to each other and the best one was selected as the initial binding complex for further modeling studies. Each of the selected best initial complex structures was energy-minimized in a similar way as performed for the energy minimization of the receptor structures, i.e., first fixing the backbone atoms of the receptor and the whole ligand structure for 2000 steps, in order to relax the side chains of the residues, especially those in the binding site. The whole complex structure was fully energy-minimized and converged at 0.01 kcal mol^{-1} Å^{-1}.

Further, to achieve the best possible "induced fit" of an agonist in the binding site of the receptor, we also carried out molecular dynamics(MD)simulations on the energy-minimizedreceptor–agonist complex structures by using the Sander module of the Amber8 program.33 We first carried out restrained MD simulations without adding additional water molecules. During the restrained MD simulations, the atoms that were allowed to move freely include those of the agonist and the residues within the binding site, including the

residues of the C-loop on the $\beta 9$ and $\beta 10$ strands (Trp174 to Thr208) and the F-loop on the complementary binding side (Gln159 to Gly172), along with the side chains of all the other residues. The complex structure was then solvated in a rectangular box of TIP3P water molecules[41] with a minimum solute–wall distance of 10 Å in order to perform MD simulations on the solvated receptor–agonist complex. 50 Na^+ and 30 Cl^- ions were randomly swapped with water molecules in order to neutralize the system and mimic the physiological condition of 0.10 M Na^+ and 0.05 M Cl^- ions. The MD-simulated system had more than 124000 atoms, e.g., 124443 atoms for the complex with **5**, including 35814 water molecules.

The solvated system was slowly heated to 300 K by weak-coupling method[42] and equilibrated for about 100 ps. During the MD simulations, a 10 Å nonbonded interaction cutoff was used and the nonbonded list was updated every 1000 steps. The particle mesh Ewald (PME) method[43] was applied to treat long-range electrostatic interactions. The lengths of bonds involving hydrogen atoms were fixed with the SHAKE algorithm,[44] enabling the use of a 2 fs time step to numerically integrate the equations of motion. Finally, the production MD simulation was kept running for ~6.5 ns with a periodic boundary condition in the NTP ensemble at $T = 300$ K with Berendsen temperature coupling and at $P = 1$ atm with anisotropic molecule-based scaling.[42] The last snapshot of the MD-simulated receptor–agonist structure was energy-minimized, and the energy-minimized structure was used as the final receptor–agonist binding structure for binding free energy calculations (see below).

Binding Free Energy Calculations

For each of the obtained receptor–agonist complex structures, the binding free energy was calculated using the scoring function developed in our previous study,[30] i.e.,

$$\Delta G_{\text{bind}} = \alpha \left(\Delta G_{\text{AD}} - E_0 \right) + \Delta G_{\text{HB}} + \Delta G_{\text{LRE}} \tag{1}$$

In eq 1, ΔG_{AD} is the binding free energy value calculated by using the standard scoring function implemented in the AutoDock 3.0.5 program[39] but excluding the contribution from hydrogen bonding. ΔG_{HB} refers to the contribution from the receptor–ligand hydrogen bonding. ΔG_{LRE} is the long-range electrostatic interaction (ΔG_{LRE}) between all of the ligand atoms and all the receptor atoms outside a 22.5 Å × 22.5 Å × 22.5 Å box (corresponding to the $60 \times 60 \times 60$ grid) centered at the mass center of the ligand. ΔG_{HB} and ΔG_{LRE} were determined by using the following equations

$$\Delta G_{\text{HB}} = \sum_{i=1}^{N} \left(\frac{\beta_{12}}{R_i^{12}} - \frac{\beta_{10}}{R_i^{10}} \right) = \beta_{12} \sum_{i=1}^{N} \frac{1}{R_i^{12}} - \beta_{10} \sum_{i=1}^{N} \frac{1}{R_i^{10}} \tag{2}$$

in which R_i was the H···O distance for the ith hydrogen bond between the ligand and the receptor;

$$\Delta G_{\text{LRE}} = \lambda \sum_{i \in R} \sum_{j \in L} \frac{q_i q_j}{\varepsilon \left(R_{ij} \right) R_{ij}} \tag{3}$$

in which R_{ij} was the internuclear distance between the ith atom (with a point charge of q_i) of the receptor and the jth atom (with a point charge of q_j) of the ligand. $\varepsilon(R_{ij})$ was the distance-

dependent dielectric constant determined by using the same function implemented in the AutoDock 3.0.5 program.[39]

In eqs 1–3, the universal empirical parameters were calibrated to be $\alpha = 0.521$, $E_0 = -2.128$, $\beta_{12} = 5.571$, $\beta_{10} = 668.580$, and $\lambda = 1.558$ in our previous study.[30]

Most of the modeling and computations were performed on a supercomputer (e.g., IBM X-series Cluster with 34 nodes and 1360 processors) at the University of Kentucky Center for Computational Sciences. Some computations were carried out on SGI Fuel workstations and a 34-processor IBM x335 Linux cluster available in our own laboratory.

Site-Directed Mutagenesis

Human α7 nAChR clone was obtained from Dr. Jon Lindstrom (University of Pennsylvania, Philadelphia, PA). The mutation of specific amino acid was introduced by means of QuikChange site-directed mutagenesis (Stratagene, La Jolla, CA). The experimental procedure was similar to that described previously.[5] Briefly, using a thermal cycler, *Pfu* DNA polymerase extended the sequence around the whole vector, generating a plasmid with staggered nicks. Each cycle built only off the parent strands; therefore there was no amplification of misincorporated bases. After 12–16 cycles, the product was treated with *Dpn I*, which digested the methylated parent DNA into numerous small pieces. The product was then transformed into *E. coli* cells, which repaired the nicks. After linearization and purification of cloned cDNAs, RNA transcripts were prepared in vitro using the appropriate mMessage mMachine kit from Ambion Inc. (Austin, TX).

Expression in *Xenopus laevis* oocytes

Mature (>9 cm) female *Xenopus laevis* African frogs (Nasco, Ft. Atkinson, WI) were used as a source of oocytes. Before surgery, the frogs were anesthetized by placing them in a 1.5 g/L solution of MS222 for 30 min. Oocytes were removed from an incision made in the abdomen.

Harvested oocytes were treated with 1.25 mg/mL collagenase (Worthington Biochemical Corporation, Freehold, NJ) for 2 h at room temperature in calcium-free Barth's solution (88 mM NaCl, 1 mM KCl, 2.38 mM $NaHCO_3$, 0.82 mM $MgS0_4$, 15 mM HEPES (pH 7.6), 12 mg/L tetracycline) in order to remove the follicular layer. Stage-5 oocytes were isolated and injected with 50 nL (5–20 ng) of each subunit cRNA. Recordings were normally conducted 2–5 days postinjection.

Electrophysiology

Experiments were conducted using Opus-Xpress6000A (Axon Instruments, Union City, CA). OpusXpress is an integrated system that provides automated impalement and voltage clamp of up to eight oocytes in parallel. Both the voltage and current electrodes were filled with 3 M KCl. The oocytes were clamped at a holding potential of −60 mV. Data were collected at 50 Hz and filtered at 20 Hz. The oocytes were bath-perfused with Ringer's solution. Agonist solutions were delivered from a 96-well plate using disposable tips. Flow rates were set at 2 mL/min.

Experimental Protocols and Data Analysis

Responses of α7 receptors were calculated as net charge.[4] Each oocyte received initial control applications of ACh, then experimental drug applications and follow-up control applications of ACh. The control ACh concentration was 300 μM. Responses to experimental drug applications were calculated relative to the preceding ACh control responses in order to normalize the data, compensating for the varying levels of channel

expression among the oocytes. Mean values and standard errors (SEM) were calculated from the normalized responses of at least four oocytes for each experimental concentration. For concentration–response relations, data derived from net-charge analyses were plotted using Kaleidagraph 3.0.2 (Abelbeck Software, Reading, PA), and curves were generated from the Hill equation

$$\text{Response} = \frac{I_{max}[\text{agonist}]^n}{[\text{agonist}]^n + [(EC_{50})^n}$$

where I_{max} denotes the maximal response for a particular agonist/subunit combination, and n represents the Hill coefficient. I_{max}, n, and the EC_{50} were all unconstrained for the fitting procedures, except in the case of the ACh response curves. Because ACh was our reference full agonist, for the ACh concentration–response curves, the data were normalized to the observed ACh maximum and the I_{max} of the curve fits were constrained to equal one.

To compare expression, oocytes harvested and injected on the same day with RNA coding for wild-type and mutant receptors were tested on the same day with the same ACh concentration. Mean responses of the mutant receptors were compared with mean responses of the wild-type receptors.

Results and Discussion

Mode of Wild-Type α7 nAChR Binding with Compounds 4 and 5

According to the energy-minimized receptor-binding structures (Figure 1A,C), the protonated tetrahydropyridyl group of **4** and **5** forms a hydrogen bond with the backbone carbonyl oxygen and a cation–π interaction with the aromatic side chain of Trp149 residue. The tetrahydropyridyl group is wrapped by several aromatic residues as Tyr93, Tyr188, Tyr195, and Trp55 from another neighboring subunit. Another pyridine group situates under the side chain of Gln117 and interacts with the disulfide bond formed by Cys190 and Cys191 in the C-loop and hydrophobic side chains of residues Leu109 and Leu119 in the complementary side of the binding site. The benzylidene group stretches toward a subsite formed by residues Tyr188 and Glu189 in the C-loop and residues Ser167, Tyr168, and Ile169 in the F-loop. The 2-methoxy group at the benzylidene structure is oriented close to the Cys190–Cys191 disulfide bond and side chain of Leu119. The 4-methoxy group of **4** packs perpendicularly with the aromatic side chain of Tyr168 and interacts with the hydrophobic side chain of Ile169 (Figure 1C). Significantly different from **4** (Figure 1C), the 4-hydroxyl group of **5** forms an O–H⋯O type of hydrogen bond with the negatively charged side chain of Glu189 (Figure 1A). Simultaneously, the OE1 atom on the side chain of Glu189 forms another hydrogen bond with the hydroxyl group on the side chain of Tyr168 in the F-loop. Such hydrogen bonding interactions between 4-hydroxyl group of **5** and residues Glu189 and Tyr168 help to improve the ligand binding with the α7 receptor. These results reveal the importance of the 4-hydroxyl group of **5** in the binding with the receptor, which explains why the binding affinity of **5** with the α7 receptor is higher than that of **4** as observed in experimental measurements.[14,18,23] Further, when the 4-hydroxyl group of **5** is replaced by a more bulky group such as −SCH₃ or −CF₃, the bulky group may bring additional steric hindrance at the local binding site. Because of the additional steric hindrance, the hydrogen bond between Glu189 and Tyr167 in the F-loop may be weakened and, as a result, the receptor may not be able to get activated (channel opening). These structural features of the obtained binding mode are consistent with the previous experimental observations, e.g., the 4-SCH3 or 4-CF3 substituted **4** had very little agonist activity and became antagonists against the α7 receptor.[18]

Our results obtained from the MD simulations also support the above-described binding mode of **5** with the α7 receptor. As shown in Figure 2, the distance between the cationic head on tetrahydropyridyl group of **5** and the backbone carbonyl oxygen of Trp149 fluctuates around 2.2 Å (black curve at the bottom panel of Figure 2) during the MD simulations, showing a hydrogen bond between the ligand and Trp149. The MD simulations also reveal a stable hydrogen bond between the 4-hydroxyl group of **5** and residue Glu189 (red curve at the bottom panel of Figure 2). Additional conformational features of the complex of **5** with the α7 receptor can be found from other tracked distances among different groups of residues. The side chain of Tyr168 forms a stable hydrogen bond with the side chain of Glu189 (blue curve at the middle panel of Figure 2), not directly hydrogen bonding with 4-hydroxyl group of **5**. The time-dependent internuclear distances also show that residue Ser167 of the F-loop is not involved in hydrogen bonding with the side chain of Glu189 and 4-hydroxyl group of the ligand, but Ser167 is close to the local binding site. These dynamic features of Ser167 and Tyr168 are consistent with the known conformational changes of the receptor after the **5** binding observed by performing site-directed labeling and fluorescence spectroscopy studies.[27,28] Using the AChBP protein as a model in those experimental studies, it was found that **5** was bound in the protonated form, i.e., the tetrahydropyridyl group was protonated. The site-directed labeling at residue Tyr164 of the F-loop of AChBP, which is in the corresponding position of Tyr168 in the α7 receptor, demonstrated that this loop had a conformational change after the agonist binding.[27,28] Such a conformational change did not happen in the antagonists binding, suggesting the coupling effects of the F-loop on the agonist binding. Interestingly, there is always a salt bridge between the side chain of Lys145 and side chain of Asp197 as the shortest distance between the charged atoms of these two residues fluctuates around 3.0 Å throughout the MD trajectory (red curve at the upper panel of Figure 2). On the other hand, Tyr188 has no direct hydrogen bonding interaction with either Lys145 or Asp197 (upper panel in Figure 2). According to the tracked distances among residues Lys145, Tyr188, and Asp197 in the MD simulations, Lys145 and Asp197 have little or no direct influences on the binding of **5** with the α7 receptor. As observed in our MD simulations, the hydroxyl group of Tyr188 is exposed to the surrounding solvent. Changing Tyr188 to a hydrophobic residue such as Phe should not be expected to affect its packing with the benzylidene group of **4** or **5**, which is consistent with the experimental observation that the Tyr188Phe or Asp197Ala mutation on the α7 receptor did not significantly change the potency of **5** with the receptor.[5]

Effects of the Gln117Phe Mutation on α7 nAChR Binding with Compounds 4 and 5

To examine how reasonable the binding mode of the α7 receptor binding with **4** and **5** is, we also modeled the Gln117Phe mutant of α7 nAChR binding with **4** and **5**. We wanted to know how important Gln117 is for α7 nAChR binding with agonists. The modeling results show that the Gln117Phe mutation has no significant influence on the orientation of **4** or **5** at the binding site (Figure 1B,D). The key hydrogen bonding distances in the Gln117Phe mutant (Figure 1B,D) are almost the same as those in the complex of the wild-type α7 receptor (Figure 1A and 1C). Using the same scoring function developed in our previous study,[30] we calculated the binding free energies (ΔG_{bind}) for the agonists binding with both wild-type α7 nAChR and its Gln117Phe mutant. The calculated ΔG_{bind} value for **4** binding with the wild-type is −8.5 kcal/mol (Table 2), close to the ΔG_{bind} value of −9.3 kcal/mol derived from the experimental K_d value (Table 1). Similarly, the ΔG_{bind} value of −10.0 kcal/mol (Table 2) calculated for **5** binding with the wild-type α7 receptor is also close to the experimentally derived ΔG_{bind} value of −10.4 kcal/mol. The ΔG_{bind} values calculated for the Gln117Phe mutant binding with **4** and **5** are nearly identical to the corresponding ΔG_{bind} values calculated for the wild-type receptor binding with **4** and **5**, within a minor difference ($\Delta\Delta G_{bind}$) of 0.1 or 0.2 kcal/mol (Table 2). These energetic results show that residue Gln117 should have no significant contribution to the binding of α7 nAChR with **4** and **5**.

Effects of the Gln117Phe Mutation on α7 nAChR Binding with 1

The structure of **1** binding with wild-type human α7 nAChR structure was modeled in our previous computational study.30 In the present study, we further computationally examined the effects of the Gln117Phe mutation on the binding of **1** based on the modeled structures for **1** binding with both the wild-type and mutant receptors. As shown in Figure 3, the Gln117Phe mutation destroyed the hydrogen bond between the side chain of Gln117 and the –NH group of **1**. Hence, the Gln117Phe mutation is expected to significantly weaken the intermolecular interaction between the ligand and receptor and, therefore, significantly decrease the binding affinity of **1** with the α7 receptor. The binding free energy calculated for **1** with the Gln117Phe mutant shows a 1.5 kcal/mol decrease in the binding affinity, i.e., $\Delta\Delta G_{bind} \equiv \Delta G_{bind}(Gln117Phe) - \Delta G_{bind}$-(wild-type)) 1.5 kcal/mol, as seen in Table 2. Concerning the accuracy of the computational predictions, in our previous computational study (using the same computational protocol)30 on a total of 14 subtype-selective agonists binding with α4β2 and α7 nAChRs, the calculated binding free energy shift ($\Delta\Delta G_{bind}$) for each of agonists was in good agreement with the binding free energy shift derived from the experimentally observed selectivity (i.e., $K_{d(\alpha4\beta2)}/K_{d(\alpha7)}$). The average deviation of the calculated relative binding free energies ($\Delta\Delta G_{bind}$) from the corresponding experimental data was ~0.6 kcal/mol, although the deviations of the calculated absolute binding free energy (ΔG_{bind}) values from the corresponding experimental ΔG_{bind} values were larger. As the same scoring function was used in the $\Delta\Delta G_{bind}$ calculations of **1** binding with both the Gln117Phe mutant and wild-type α7 receptors, the calculated $\Delta\Delta G_{bind}$ value of 1.5 kcal/mol suggests that Gln117 residue indeed has a significant contribution to the binding of **1** with the α7 receptor, although the predicted decrease in binding affinity is not dramatic.

Effects of the Gln117Phe Mutation on α7 nAChR Binding with Compounds 2 and 3

To better understand α7 nAChR binding with **1**, we also modeled α7 nAChR binding with two analogues (compounds **2** and **3** in Table 1) of **1** and calculated the ΔG_{bind} values for their binding with wild-type α7 nAChR and its Gln117Phe mutant. Depicted in Figure 4 are the obtained binding structures. The orientations of compounds **2** and **3** in the binding site are essentially the same as that of compound **1**. A remarkable difference exists in the hydrogen bonding with the side chain of Gln117. Going from compound **1** to **2** or **3**, the hydrogen atom on the carbamate nitrogen is replaced by a methyl ($-CH_3$) or ethyl ($-CH_2CH_3$) group. As a result, compounds **2** and **3** do not have a $-NH$ group available to form a hydrogen bond with the side chain of Gln117 like **1**, which explains why the binding affinities of **2** and **3** are lower than that of **1** (see Table 2). The calculated binding free energies (Table 2) are qualitatively consistent with the available experimental data for their binding with the wild-type receptor. It is interesting to note that the binding free energies calculated for compounds **2** and **3** binding with the Gln117Phe mutant are all lower than the corresponding binding free energies calculated for their binding with the wild-type. These two compounds have a higher binding affinity with the Gln117Phe mutant compared to the wild-type receptor because the Gln117Phe mutation changes the hydrophilic side chain of Gln117 to the hydrophobic side chain of Phe and, thus, make the amino acid residue at position no. 117 of the receptor more compatible with the hydrophobic functional group ($-CH_3$ or $-CH_2CH_3$) on the carbamate nitrogen of the ligand. Hence, the Gln117Phe mutation helps to make a favorable hydrophobic interaction between the ligand and residue no. 117 of the receptor. The larger the hydrophobic functional group ($-CH_3$ or $-CH_2CH_3$) on the carbamate nitrogen of the ligand, the larger the calculated change ($\Delta\Delta G_{bind}$) of the binding free energy is. As seen in Table 2, the $\Delta\Delta G_{bind}$ value calculated for compound **2** (with $-CH_3$ on the carbamate nitrogen) is −1.0 kcal/mol, and the $\Delta\Delta G_{bind}$ value calculated for compound **3** (with $-CH_2CH_3$ on the carbamate nitrogen) is −2.2 kcal/mol.

Wet Experimental Tests on the Computational Predictions

It is important to test and validate the binding insights obtained from the computational modeling. The aforementioned computational results have led to some interesting predictions of the effects of the Gln117Phe mutation on the agonists binding with α7 nAChR. Particularly, the computational modeling predicts that the receptor–agonist binding mode for **4** and **5** is significantly different from that for **1** and its analogues and that the Gln117Phe mutation differentially affects the binding of different agonists: (1) the Gln117Phe mutation will not significantly change the binding affinities of **4** and **5**, (2) the Gln117Phe mutation will significantly decrease the binding affinity of **1**, (3) the Gln117Phe mutation will significantly increase the binding affinities of the two **1** analogues (compounds **2** and **3**). The predictions for the effects of the Gln117Phe mutation are testable. To test some of these predictions, we made the Gln117Phe mutant of human α7 nAChR through site-directed mutagenesis and carried out electrophysiological tests on the mutant and wild-type receptors with both **1** and **5** (the two practically interesting compounds that are actually available to us). The detailed experimental studies will be reported elsewhere. Here, for the purpose of validation of computational predictions, we only present and discuss the major results obtained from the electrophysiological measurements.

It should be pointed out that the measured EC_{50} values reflect the overall agonist functions (associated with the channel opening) of the agonists and cannot be compared directly to the predicted binding affinities of the agonists with the receptors. This is because, in binding experiments, the prolonged exposure of the receptor to ligand promotes conversion of the receptors to desensitized states that retain the agonist binding sites in altered conformations most likely related to those associated with activated channels. However, mutations that affect the efficacy of multiple agonists may also shift the basic equilibrium between the active and desensitized states. It should be noted that on the average the maximal ACh response of the α7 Gln117Phe mutant nAChR was only 30% compared to wild-type α7 receptor (data not shown). As the Gln117Phe mutation is not expected to significantly change the α7 receptor binding with ACh,[25,45] the decrease of the maximal ACh response of the α7 Gln117Phe mutant nAChR could be attributed to the possible mutation-caused shift of the basic equilibrium between the active and desensitized states. Theoretically, a specific mutation may or may not similarly shift the basic equilibrium for different agonists. When the Gln117Phe mutation can similarly shift the basic equilibrium for both the reference (ACh) and an agonist (**1** or **5**) under consideration, the responses of the mutant receptor to the agonist relative to the maximal ACh responses of the same mutant should not be affected significantly by the similar basic equilibrium shift. Assuming that this is the case for the Gln117Phe mutation and agonists (**1** and **5**) under consideration here, when the mutation does not significantly affect the binding affinity of an agonist, the mutation should also not significantly change the corresponding EC_{50} value. When the mutation significantly decreases/increases the binding affinity of an agonist, the mutation should also significantly decrease/increase the corresponding EC_{50} value.

Depicted in Figure 5 are the obtained electrophysiological data for the agonist functions of **1** and **5** with the wild-type α7 nAChR and its Gln117Phe mutant relative to the reduced maximal ACh responses. The data in Figure 5A show that the EC_{50} value of **5** was $3.0 \pm 0.26\ \mu M$ for the wild-type α7 nAChR and $5.2 \pm 0.84\ \mu M$ for the Gln117Phe mutant. The change of the measured EC_{50} value corresponding to the Gln117Phe mutation was insignificant, which qualitatively supports the computational prediction that the Gln117Phe mutation would not significantly affect the binding of agonist **5** with the α7 receptor.

The data in Figure 5B reveal that the EC_{50} value of **1** was $3.6 \pm 0.73\ \mu M$ for the wild-type α7 nAChR and $22.3 \pm 1.31\ \mu M$ for the Gln117Phe mutant. The Gln117Phe mutation increased the EC_{50} value of compound **1** by ~6.2-fold. The ~6.2-fold increase of the EC_{50}

value is significant, which qualitatively supports the computational prediction that the Gln117Phe mutation will significantly decrease the binding affinity of compound **1**. If the ~6.2-fold increase in the potency is associated with >6.2-fold increase in the binding affinity, this >6.2-fold increase in the affinity would correspond to >1.1 kcal/mol decrease in the binding free energy, i.e., $\Delta\Delta G_{expt} \equiv \Delta G_{expt}(\text{Gln117Phe}) - \Delta G_{expt}(\text{wild-type}) = <-1.1$ kcal/mol for compound **1**. The $\Delta\Delta G_{expt}$ value of <-1.1 kcal/mol is consistent with the predicted $\Delta\Delta G_{bind}$ value of -1.5 kcal/mol.

The satisfactory agreement between the experimental data and computational predictions suggests that the receptor–agonist binding modes and structure–activity insights obtained from the computational modeling are reliable.

Conclusion

Our computational modeling and simulations have revealed how α7-specific agonists of nAChR, including **4** and **5**, could interact with the α7 receptor. According to the determined binding mode, the cationic head of **4** and **5** has favorable hydrogen bonding and cation–π interactions with residue Trp149 of the receptor. In addition, **4** and **5** also interact with the subsite formed by residues in the C-loop on the principal side of the binding site and the residues Ser167, Tyr168, and Ile169 in the F-loop on the neighboring subunit. These residues from the F-loop are coupled with agonist binding, through the hydrogen bonding of the hydroxyl group on the side chain of Tyr168 with the side chain of Glu189 in the C-loop. The 4-hydroxyl group of **5** acts as a hydrogen bonding donor to form a hydrogen bond with side chain of Glu189 and thus increases its binding affinity with the receptor. The calculated relative binding free energies of **4** and **5** are qualitatively consistent with available experimental observations.

The computational results have also led us to better understand the roles of Gln117 and other residues in the α7 receptor binding with agonists. On the basis of the computational modeling, the Gln117Phe mutation should not significantly change the binding affinities of **4** and **5** but should significantly decrease the binding affinity of **1** and significantly increase the binding affinities of compounds **2** and **3**. The computational predictions are supported by data obtained from wet experimental tests on two available compounds, i.e., **1** and **5**, with both wild-type α7 receptor and its Gln117Phe mutant. The wet experimental data confirm that the Gln117Phe mutation does not significantly change the EC_{50} value of **5** but does significantly increase the EC_{50} value of **1**.

The new insights into the receptor–agonist binding and structure–activity relationship obtained from this study should be valuable for future rational design of more potent and selective agonists of the α7 receptor. For example, our modeled binding structures reveal that the important receptor–agonist interactions include the hydrogen bonding and cation–π interactions between the cationic head of the agonist and Trp149 (for all of the examined α7-specific agonists) plus the hydrogen bonding of the agonists with residue Gln117 (for **1**) or Glu189 (for **5**). Because these favorable interactions are crucial for the receptor binding with α7-specific agonists **1** or **5**, one may consider designing possibly more potent and selective new agonists that can have the similar (or stronger) favorable interactions with all of these important residues, i.e., Gln117, Trp149, and Glu189 of the α7 receptor.

Supplementary Material

Refer to Web version on PubMed Central for supplementary material.

Acknowledgments

References

(1). Lester HA, Dibas MI, Dahan DS, Leite JF, Dougherty DA. Cys-loop receptors: new twists and turns. Trends Neurosci. 2004; 27:329–336. [PubMed: 15165737]

(2). Jensen AA, Frolund B, Liljefors T, Krogsgaard-Larsen P. Neuronal nicotinic acetylcholine receptors: structural revelations, target identifications, and therapeutic inspirations. J. Med. Chem. 2005; 48:4705–4745. [PubMed: 16033252]

(3). Kempsill FEJ, Covernton PJO, Whiting PJ, Connolly JG. Agonist activation and a-bungarotoxin inhibition of wild type and mutant a7 nicotinic acetylcholine receptors. Eur. J. Pharmacol. 1999; 383:347–359. [PubMed: 10594329]

(4). Papke RL, Papke JKP. Comparative pharmacology of rat and human a7 nAChR conducted with net charge analysis. Br. J. Pharmacol. 2002; 137:49–61. [PubMed: 12183330]

(5). Horenstein NA, McCormack TJ, Stokes C, Ren K, Papke RL. Reversal of agonist selectivity by mutations of conserved amino acids in the binding site of nicotinic acetylcholine receptors. J. Biol. Chem. 2007; 282:5899–5909. [PubMed: 17189260]

(6). Galzi J-L, Bertrand D, Devillers-Thiery A, Revah F, Bertrand S, Changeus J-P. Functional significance of aromatic amino acids from three peptide loops of the a7 neuronal nicotinic receptor site investigated by site-directed mutagenesis. FEBS Lett. 1991; 294:198–202. [PubMed: 1756861]

(7). Kem WR. The brain a7 nicotinic receptor may be an important therapeutic target for the treatment of Alzheimer's disease: studies with DMXBA (GTS-21). Behav. Brain Res. 2000; 113:169–181. [PubMed: 10942043]

(8). Lyford LK, Sproul AD, Eddins D, Mclaughlin JT, Rosenberg RL. Agonist-induced conformational changes in the extracellular domain of α7 nicotinic acetylcholine receptors. Mol. Pharm. 2003; 64:650–658.

(9). Cao Y-J, Surowy CS, Puttfarcken PS. Different nicotinic acetylcholine receptor subtypes mediating striatal and prefrontal cortical [3H]dopamine release. Neuropharmacology. 2005; 48:72–79. [PubMed: 15617729]

(10). Grassi F, Palma E, Tonini R, Amici M, Ballivet M, Eusebi F. Amyloid β1-42 peptide alters the gating of human and mouse α-bungarotoxin-sensitive nicotinic receptors. J. Physiol. 2003; 547:147–157. [PubMed: 12562926]

(11). Fischer H, Liu D-M, Lee A, Harries JC, Adams DJ. Selective modulation of neuronal nicotinic acetylcholine receptor channel subunits by Go-protein subunits. J. Neurosci. 2005; 25:3571–3577. [PubMed: 15814787]

(12). Mullen G, Napier J, Balestra M, DeCory T, Hale G, Macor J, Mack R, Loch J, Wu E, Kover A, Verhoest P, Sampognaro A, Phillips E, Zhu Y, Murray R, Griffith R, Blosser J, Curley D, Machulskis A, Zongrone J, Rosen A, Gordon J. (−)-Spiro[1-azabicyclo[2.2.2]octane-3,5′-oxazolidin-2′-one], a conformationally restricted analogue of acetylcholine, is a highly selective full agonist at the α7 nicotinic acetylcholine receptor. J. Med. Chem. 2000; 43:4045–4050. [PubMed: 11063601]

(13). Kampen M, Selbach K, Schneider R, Schiegel E, Boess F, Schreiber R. AR-R 17779 improves social recognition in rats by activation of nicotinic α7 receptors. Psychopharmacology (Berlin). 2004; 172:375–383. [PubMed: 14727003]

(14). De Fiebre CM, Meyer EM, Henry JC, Muraskin SI, Kem WR, Papke RL. Characterization of a series of anabaseine-derived compounds reveals that the 3-(4)-dimethylaminocinnamylidine derivative is a selective agonist at neuronal nicotinic a7/^{125}I-a-bungarotoxin receptor subtypes. Mol. Pharmacol. 1996; 47:164–171. [PubMed: 7838125]

(15). Briggs CA, Anderson DJ, Brioni JD, Buccafusco JJ, Buckley MJ, Campbell JE, Decker MW, Donnelly-Roberts D, Elliott RL, Gopalakrishnan M, Holladay MW, Hui YH, Jackson WJ, Kim DJ, Marsh KC, O'Neill A, Prendergast MA, Ryther KB, Sullivan JP, Arneric SP. Functional characterization of the novel neuronal nicotinic acetylcholine receptor ligand GTS-21 in vitro and in vivo. Pharmacol., Biochem. Behav. 1997; 57:231–241. [PubMed: 9164577]

(16). Haaren FV, erson KG, Haworth SC, Kem WR. GTS-21, a mixed nicotinic receptor agonist/antagonist, does not affect the nicotine cure. Pharmacol., Biochem. Behav. 1999; 64:439–444. [PubMed: 10515327]

(17). Stokes C, Papke JKP, Horenstein NA, Kem WR, McCormack TJ, Papke RL. The structural basis for GST-21 selectivity between human and rat nicotinic a7 receptors. Mol. Pharmcol. 2004; 66:14–24.

(18). Papke RL, Meyer EM, Lavieri S, Bollampally SR, Papke TAS, Horenstein NA, Itoh Y, Papke JKP. Effects at a distance in a7 nAChR selective agonists: benzylidene substitutions that regulate potency and efficacy. Neuropharmacology. 2004; 46:1023–1038. [PubMed: 15081799]

(19). Arendash GW, Sengstock GJ, Sanberg PR, Kem WR. Improved learning and memory in aged rats with chronic administration of the nicotinic receptor agonist GTS-21. Brain Res. 1995; 674:252–259. [PubMed: 7796104]

(20). Uteshev VV, Meyer EM, Papke RL. Regulation of neuronal function by choline and 4OH-GTS-21 through a7 nicotinic receptors. J. Neurophysiol. 2003; 89:1797–1806. [PubMed: 12611953]

(21). Ren K, King MA, Liu J, Siemann J, Altman M, Meyers C, Hughes JA, Meyer EM. The a7 nicotinic receptor agonist 4OH-GTS-21 protects axotomized septohippocampal cholinergic neurons in wild type but not amyloid-overexpressing transgenic mice. Neuroscience. 2007; 148:230–237. [PubMed: 17640819]

(22). Kem WR, Mahnir VM, Prokai L, Papke RL, Cao X, LeFrancois S, Wildeboer K, Prokai-Tatrai K, Porter-Papke J, Soti F. Hydroxy metabolites of the Alzheimer's drug candidates 3-[(2,4-dimethoxy) benzylidene]-anabaseine dihydrochloride (GTS-21): their molecular properties, interactions with brain nicotinic receptors, and brain penetration. Mol. Pharmacol. 2004; 65:56–67. [PubMed: 14722237]

(23). Unwin N. Refined structure of the nicotinic acetylcholine receptor at 4 Å resolution. J. Mol. Biol. 2005; 346:967–989. [PubMed: 15701510]

(24). Dellisanti C, Yao Y, Stroud J, Wang Z-Z, Chen L. Crystal structure of the extracellular domain of nAChR a1 bound to a-bungarotoxin at 1.94 Å resolution. Nat. Neurosci. 2007; 10:953–962. [PubMed: 17643119]

(25). Celie PHN, Rossum-Fikkert SE, Dijk WJ, Brejc K, Smit AB, Sixma TK. Nicotine and carbamylcholine binding to nicotinic acetylcholine receptors as studied in AChBP crystal structures. Neuron. 2004; 41:907–914. [PubMed: 15046723]

(26). Hansen SB, Sulzenbacher G, Huxford T, Marchot P, Taylor P, bourne Y. Structure of aplysia AChBP complexes with nicotine agonists and antagonists revealed distinctive binding interfaces and conformations. EMBO J. 2005; 24:3635–3646. [PubMed: 16193063]

(27). Talley TT, Yalda S, Ho K-Y, Tor Y, Soti FS, Kem WR, Taylor P. Spectroscopic analysis of benzylidene anabaseine complexes with acetylcholine binding proteins as models for ligand–nicotinic receptor interactions. Biochem. 2006; 45:8894–8902. [PubMed: 16846232]

(28). Hibbs R, Radic Z, Taylor P, Johnson DA. Influence of agonists and antagonists on the segmental motion of residues near the agonist binding pocket of the acetylcholine-binding protein. J. Biol. Chem. 2006; 281:39708–39718. [PubMed: 17068341]

(29). Huang X, Zheng F, Crooks PA, Dwoskin LP, Zhan C-G. Modeling multiple species of nicotine and deschloroepibatidine interacting with $\alpha 4\beta 2$ nicotinic acetylcholine receptor: from microscopic binding to phenomenological binding affinity. J. Am. Chem. Soc. 2005; 127:14401–14414. [PubMed: 16218635]

(30). Huang X, Zheng F, Chen X, Crooks PA, Dwoskin LP, Zhan C-G. Modeling subtype-selective agonists binding with $\alpha 4\beta 2$ and $\alpha 7$ nicotinic acetylcholine receptors: effects of local binding and long-range electrostatic interactions. J. Med. Chem. 2006; 49:7661–7674. [PubMed: 17181149]

(31). Residue numbering is based on the α7 nAChR clone originally from Dr. Jim Boulter (UCLA, Los Angeles, CA). Accordingly, the residue numbering in refs 29 and 30 should be corrected for both α7 and α4β2 nAChRs: the previous Trp148 of α7 nAChR is now Trp149; the previous αTrp147 of α4β2 nAChR is now αTrp149; the previous βTrp53 is now βTrp55; and so on for others.

(32). Frisch, MJ.; Trucks, GW.; Schlegel, HB.; Scuseria, GE.; Robb, MA.; Cheeseman, JR.; Montgomery, JA., Jr.; Vreven, T.; Kudin, KN.; Burant, JC.; Millam, JM.; Iyengar, SS.; Tomasi, J.; Barone, V.; Mennucci, B.; Cossi, M.; Scalmani, G.; Rega, N.; Petersson, GA.; Nakatsuji, H.; Hada, M.; Ehara, M.; Toyota, K.; Fukuda, R.; Hasegawa, J.; Ishida, M.; Nakajima, T.; Honda, Y.; Kitao, O.; Nakai, H.; Klene, M.; Li, X.; Knox, JE.; Hratchian, HP.; Cross, JB.; Adamo, C.; Jaramillo, J.; Gomperts, R.; Stratmann, RE.; Yazyev, O.; Austin, AJ.; Cammi, R.; Pomelli, C.; Ochterski, JW.; Ayala, PY.; Morokuma, K.; Voth, GA.; Salvador, P.; Dannenberg, JJ.; Zakrzewski, VG.; Dapprich, S.; Daniels, AD.; Strain, MC.; Farkas, O.; Malick, DK.; Rabuck, AD.; Raghavachari, K.; Foresman, JB.; Ortiz, JV.; Cui, Q.; Baboul, AG.; Clifford, S.; Cioslowski, J.; Stefanov, BB.; Liu, G.; Liashenko, A.; Piskorz, P.; Komaromi, I.; Martin, RL.; Fox, DJ.; Keith, T.; Al-Laham, MA.; Peng, CY.; Nanayakkara, A.; Challacombe, M.; Gill, PMW.; Johnson, B.; Chen, W.; Wong, MW.; Gonzalez, C.; Pople, JA. *Gaussian 03*, Revision A. 1. Gaussian, Inc.; Pittsburgh, PA: 2003.

(33). Case, DA.; Darden, TA., III; Cheatham, TE.; Simmerling, CL.; Wang, J.; Duke, RE.; Luo, R.; Merz, KM.; Wang, B.; Pearlman, DA.; Crowley, M.; Brozell, S.; Tsui, V.; Gohlke, H.; Mongan, J.; Hornak, V.; Cui, G.; Beroza, P.; Schafmeister, C.; Caldwell, JW.; Ross, WS.; Kollman, PA. Amber 8. University of California; San Francisco, CA: 2004.

(34). (a) Zhan C-G, Zheng F, Landry DW. Fundamental reaction mechanism for cocaine hydrolysis in human butyrylcholinesterase. J. Am. Chem. Soc. 2003; 125:2462–2474. [PubMed: 12603134] (b) Pan Y, Gao D, Yang W, Cho H, Yang G-F, Tai H-H, Zhan C-G. Computational redesign of human butyrylcholinesterase for anti-cocaine medication. Proc. Natl. Acad. Sci. U.S.A. 2005; 102:16656–16661. [PubMed: 16275916] (c) Pan Y, Gao D, Yang W, Cho H, Zhan C-G. Free energy perturbation (FEP) simulation on the transition states of cocaine hydrolysis catalyzed by human butyrylcholinesterase and its mutants. J. Am. Chem. Soc. 2007; 129:13537–13543. [PubMed: 17927177]

(35). Huang X, Yan W, Gao D, Tong M, Tai H-H, Zhan C-G. Structural and functional characterization of human microsomal prostaglandin E synthase-1 (mPGES-1) by computational modeling and site-directed mutagenesis. Bioorg. Med. Chem. 2006; 14:3553–3562. [PubMed: 16439136]

(36). Huang X, Zhan C-G. How dopamine transporter interacts with dopamine: insights from molecular modeling and simulation. Biophys. J. 2007; 93:3627–3639. [PubMed: 17704152]

(37). (a) Pan Y, Gao D, Zhan C-G. Modeling the catalysis of anti-cocaine catalytic antibody: competing reaction pathways and free energy barriers. J. Am. Chem. Soc. 2008; 130:5140–5149. [PubMed: 18341277] (b) Zheng F, Yang W, Ko M-C, Liu J, Cho H, Gao D, Tong M, Tai H-H, Woods JH, Zhan C-G. Most efficient cocaine hydrolase designed by virtual screening of transition states. J. Am. Chem. Soc. 2008; 130:12148–12155. [PubMed: 18710224] (c) Hamza A, Abdul Hameed MDM, Zhan C-G. Understanding microscopic binding of human microsomal prostaglandin E synthase-1 with substrates and inhibitors by molecular modeling and dynamics simulation. J. Phys. Chem. B. 2008; 112:7320–7329. [PubMed: 18476739]

(38). Zhang T, Hamza A, Cao X, Wang B, Yu S, Zhan C-G, Sun D. A novel Hsp90 inhibitor disrupts Hsp90/Cdc37 complex for pancreatic cancer therapy. Mol. Cancer Ther. 2008; 7:162–170. [PubMed: 18202019]

(39). Morris GM, Goodsell DS, Halliday RS, Huey R, Hart WE, Belew RK, Olson AJ. Automated docking using a Lamarckian genetic algorithm and empirical binding free energy function. J. Comput. Chem. 1998; 19:1639–1662.

(40). Solis FJ, Wets RJB. Minimization by random search techniques. Math. Oper. Res. 1981; 6:19–30.

(41). Jorgensen WL, Chandrasekhar J, Madura JD, Impey RW, L. KM. Comparison of Simple Potential Functions for Simulating Liquid Water. J. Chem. Phys. 1983; 79:926–935.

(42). Berendsen HJC, Postma JPM, van Gunsteren WF, DiNola A, Haak JR. Molecular dynamics with coupling to an external bath. J. Chem. Phys. 1984; 81:3684–3690.

(43). Toukmaji A, Sagui C, Board CJ, Darden T. Efficient particle-mesh Ewald based approach to fixed and induced dipolar interactions. J. Chem. Phys. 2000; 113:10913–10927.

(44). Ryckaert JP, Ciccotti G, Berendsen HJC. Numerical integration of the Cartesian equations of motion of a system with constraints: Molecular dynamics of *n*-alkanes. J. Comput. Phys. 1977; 23:327–341.

(45). Assuming that the receptor-ACh binding mode is similar to the AChBP–carbamylcholine binding mode in the X-ray crystal structure reported in ref 25. ACh is expected to be far away from Gln117 of the α7 receptor.
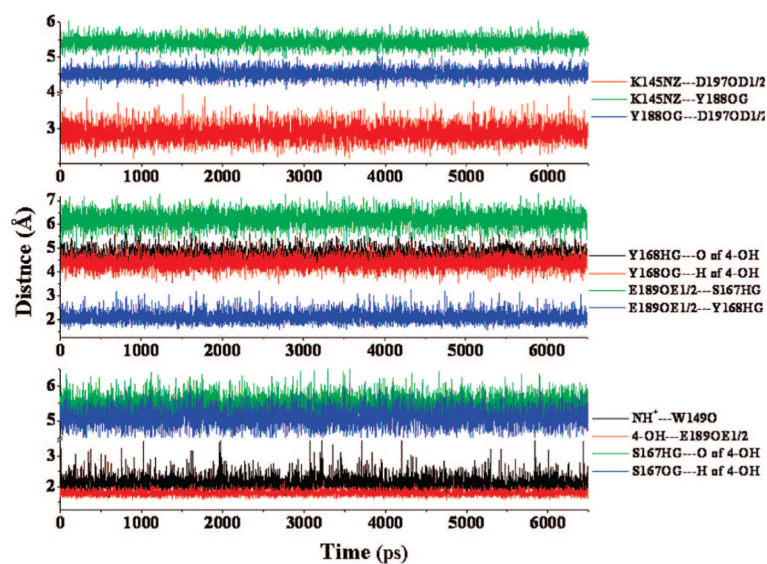
Figure 1.
Molecular interactions between agonists and α7 nAChR. Residues of the receptor are labeled and shown in stick, whereas the agonist molecules are shown in ball-and-stick. Hydrogen bonding interactions are indicated by dashed lines with the key distances. (A) compound **5** with wild-type α7 nAChR. (B) **5** with the Gln117Phe mutant. (C) **4** with wild-type α7 nAChR. (D) **4** with the Gln117Phe mutant.

Figure 2.
Time-dependence of the key distances for the complex of compound **5** with α7 nAChR during the molecular dynamics simulations. NH$^+$ represents the proton at the cationic head of **5**, and 4-OH refers to the 4-hydroxyl group of **5**.
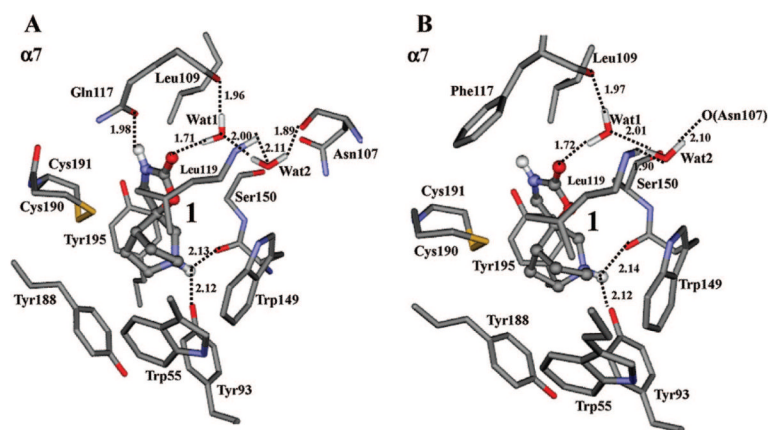
Figure 3.
Compound **1** binding with wild-type α7 nAChR (A) and its Gln117Phe mutant (B). Residues of the receptor are represented in stick and **1** in ball-and-stick. Important hydrogen bonding interactions are shown in dashed lines with key distances.
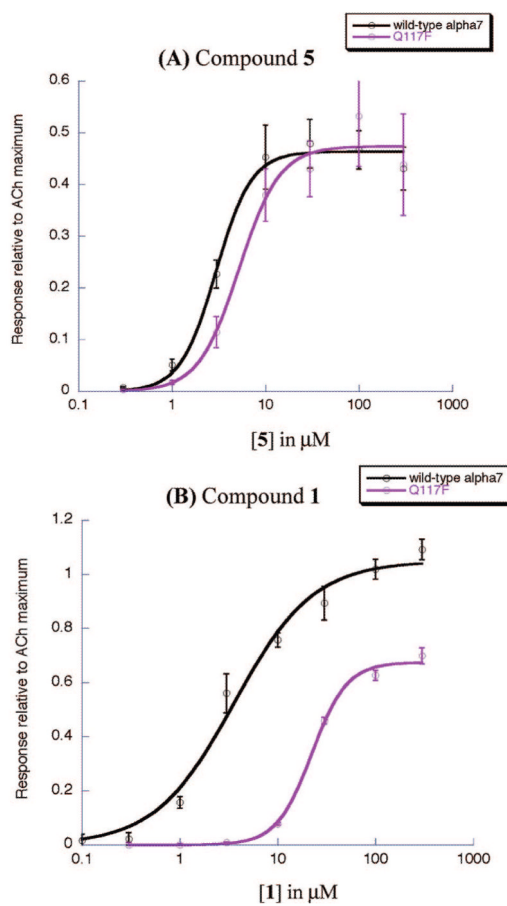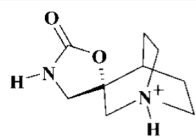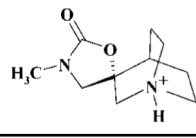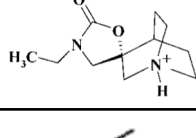
Figure 4.
Molecular interactions of compounds **2** and **3** with wild-type α7 nAChR and its Gln117Phe mutant. Residues of the receptor are shown as stick, whereas compounds **2** and **3** are shown in ball-and-stick. Key hydrogen bonding distances are indicated. (A) Compound **2** with the wild-type receptor. (B) Compound **2** with the Gln117Phe mutant. (C) Compound **3** with the wild-type receptor. (D) Compound **3** with the Gln117Phe mutant.
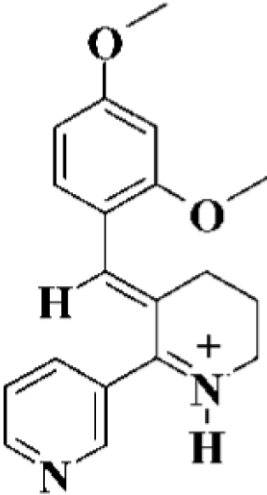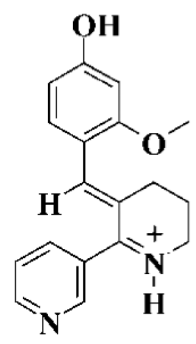
Figure 5.
Agonist concentration response data for wild-type and Gln117Phe mutant α7 receptors: (A) compound **5**; (B) compound **1**.

Table 1

Protonated Molecular Structures of Compounds **1**–**5**, along with Their Experimental Binding Affinities (K_d) with α7 nAChR

Ligand	Molecular structure	K_d (nM)	Ref
1		92 ± 10	12, 13
2		220 ± 60	12
3		690 ± 20	12
4		158	14, 23
5		23	23

Table 2

Binding Free Energies (in kcal/mol) Calculated for Agonists with $\alpha 7$ nAChR in Comparison with the Experimentally Derived Binding Free Energies

ligand	receptor	$a(\Delta G_{AD}\text{-}E0)$	ΔG_{HB}	ΔG_{LRE}	ΔG_{bind}	$\Delta\Delta G_{bind}{}^{a}$	$\Delta G_{expt}{}^{b}$
1	WT	−2.52	−4.60	−4.77	−11.9	1.5	−9.6
	Gln117Phe	−2.65	−3.72	−4.03	−10.4		
2	WT	−3.19	−2.69	−4.23	−10.1	−1.0	−9.1
	Gln117Phe	−3.24	−3.71	−4.13	−11.1		
3	WT	−3.25	−1.87	−4.28	−9.4	−2.2	−8.4
	Gln117Phe	−3.20	−3.88	−4.54	−11.6		
4	WT	−3.81	−0.46	−4.21	−8.5	−0.2	−9.3
	Gln117Phe	−3.98	−0.47	−4.22	−8.7		
5	WT	−3.83	−1.71	−4.45	−10.0	−0.1	−10.4
	Gln117Phe	−4.01	−1.63	−4.43	−10.1		

[a] The shift of the calculated ΔG_{bind} value caused by the Gln117Phe mutation, i.e., $\Delta\Delta G_{bind} \equiv \Delta G_{bind}(\text{Gln117Phe}) - \Delta G_{bind}(\text{wild-type})$.

[b] Binding free energy derived from experimental dissociation constant (K_d) values collected in Table 1 via $\Delta G_{bind} = RT \times \ln K_d$.